Plant Physiology®

Research Article

The plant POLYMERASE-ASSOCIATED FACTOR1 complex links transcription and H2B monoubiquitination genome wide

Noel Blanco-Touriñán [ID],[1,†] Jaime Pérez-Alemany [ID],[1,†] Clara Bourbousse [ID],[2] David Latrasse [ID],[3] Ouardia Ait-Mohamed [ID],[2] Moussa Benhamed [ID],[3] Fredy Barneche [ID],[2] Miguel A. Blázquez [ID],[1] Javier Gallego-Bartolomé [ID][1] and David Alabadí [ID][1,*]

1   Instituto de Biología Molecular y Celular de Plantas (CSIC-UPV), 46022 Valencia, Spain
2   Ecole Normale Supérieure, Institut de Biologie de l'Ecole Normale Supérieure (CNRS), CNRS, INSERM, Université PSL, 75230 Paris, France
3   Institute of Plant Sciences Paris-Saclay (Université Paris-Saclay-CNRS), 91190 Gif-sur-Yvette, France

*Author for correspondence: dalabadi@ibmcp.upv.es
†These authors contributed equally.
The author responsible for distribution of materials integral to the findings presented in this article in accordance with the policy described in the Instructions for Authors (https://academic.oup.com/plphys/pages/General-Instructions) is: David Alabadí.

Abstract

The evolutionarily conserved POLYMERASE-ASSOCIATED FACTOR1 complex (Paf1C) participates in transcription, and research in animals and fungi suggests that it facilitates RNA POLYMERASE II (RNAPII) progression through chromatin. We examined the genomic distribution of the EARLY FLOWERING7 (ELF7) and VERNALIZATION INDEPENDENCE3 subunits of Paf1C in Arabidopsis (*Arabidopsis thaliana*). The occupancy of both subunits was confined to thousands of gene bodies and positively associated with RNAPII occupancy and the level of gene expression, supporting a role as a transcription elongation factor. We found that monoubiquitinated histone H2B, which marks most transcribed genes, was strongly reduced genome wide in *elf7* seedlings. Genome-wide profiling of RNAPII revealed that in *elf7* mutants, RNAPII occupancy was reduced throughout the gene body and at the transcription end site of Paf1C-targeted genes, suggesting a direct role for the complex in transcription elongation. Overall, our observations suggest a direct functional link between Paf1C activity, monoubiquitination of histone H2B, and the transition of RNAPII to productive elongation. However, for several genes, Paf1C may also act independently of H2Bub deposition or occupy these genes more stable than H2Bub marking, possibly reflecting the dynamic nature of Paf1C association and H2Bub turnover during transcription.

Introduction

During gene transcription, numerous proteins and protein complexes help RNA POLYMERASE II (RNAPII) to move through the gene body, including histone chaperones, chromatin remodelers, and transcription elongation factors, most of which are evolutionarily conserved in eukaryotes (Obermeyer, Kapoor, et al. 2023). One of them is the transcription elongation complex POLYMERASE-ASSOCIATED FACTOR1 complex (Paf1C). Paf1C was originally identified in yeast (*Saccharomyces cerevisiae*), and the current view of how Paf1C acts in gene regulation is largely based on studies in yeast and mammals (Francette et al. 2021). Early genetic and biochemical evidence for a positive role of Paf1C in transcriptional elongation (Shi et al. 1997; Rondón et al. 2004) is now supported by structural studies showing the association of the complex with active RNAPII (Vos et al. 2018; Vos et al.

Open Access

2020). Paf1C is also involved in posttranslational modification of histones. Histone modifications such as the monoubiquitination of histone H2B (H2Bub) or the methylation of lysine 4 or 36 of histone H3 (H3K4me and H3K36me), which influence chromatin dynamic cotranscriptionally to facilitate RNAPII progression, have been found to be dependent on Paf1C in yeast and mammals (Francette et al. 2021).

Several subunits of plant Paf1C have been genetically identified in Arabidopsis (*Arabidopsis thaliana*) in genetic screens for early flowering mutants or by searching for homologous genes (Zhang and Van Nocker 2002; Zhang et al. 2003; He et al. 2004; Oh et al. 2004; Park et al. 2010; Yu and Michaels 2010). As in animals, the plant Paf1C contains 6 subunits: PLANT HOMOLOGOUS TO PARAFIBROMIN (PHP)/CELL DIVISION CYCLE73 (CDC73), VERNALIZATION INDEPENDENCE2 (VIP2; also known as EARLY FLOWERING7 [ELF7]), VIP3, VIP4, VIP5, and VIP6 (ELF8), which are the putative orthologs of CDC73, Paf1, SUPERKILLER8, LEFT OPEN READING FRAME1, RESTORES TBP FUNCTION1, and CLN THREE REQUIRING9, respectively (Obermeyer, Kapoor, et al. 2023). The Arabidopsis Paf1C is formed in vivo since at least VIP3, VIP4, and VIP6 interact with PHP/CDC73 (Park et al. 2010), and all subunits were identified in interactomic analyses using CDC73 and ELF7 as baits (Antosz et al. 2017). Furthermore, the latter study showed that Paf1C interacts with bona fide transcriptional elongation factors and with several subunits of RNAPII, pointing to a conserved role in transcriptional elongation.

In addition to flowering, and consistent with the pleiotropic effects of loss-of-function mutants in several subunits, plant Paf1C has been associated genetically with a variety of largely unrelated physiological processes in Arabidopsis, including seed dormancy (Liu et al. 2011), shoot apical meristem activity (Fal et al. 2017; Fal et al. 2019; Li et al. 2022), thermomorphogenesis (Zhao et al. 2023), and the response to salt stress (Zhang et al. 2022) and DNA damaging agents (Li et al. 2023).

In Arabidopsis, the role of Paf1C in posttranslational modification of histones is well documented and has been associated with several physiological processes. This includes the regulation of flowering time by acting on the flowering repressor gene FLOWERING LOCUS C (*FLC*) and its paralogs (Cao et al. 2015; Lu et al. 2017; Li et al. 2019; Nasim et al. 2022). The requirement of Paf1C for histone modifications has also been shown at the epigenomic level. Although the total amount of H3K4me3 and H3K36me2 marks is not altered in *vip3*, *vip4*, *vip5*, or *vip6* cell extracts (Oh et al. 2004), the *vip3* mutation triggers a slight redistribution of both marks across gene bodies (Oh et al. 2008). Moreover, plant Paf1 subunits are required for the correct distribution of H2A.Z and H3.3 in response to warm temperatures (Zhao et al. 2023) and for regulating H3K27 trimethylation at a subset of genes (Oh et al. 2008; Schmitz et al. 2009).

In line with the role of Paf1C in animals and fungi in promoting H2Bub accumulation, mutations in Arabidopsis VIP2, VIP4, VIP5, and VIP6 subunits cause decreased H2Bub accumulation at *FLC* and its paralog genes (Cao et al. 2015). More recently, the dependence of H2Bub on Paf1C has been linked to the DNA damage response (Li et al. 2023). In Arabidopsis, as in yeast and animals, H2Bub accumulates across the gene bodies of actively transcribed genes (Roudier et al. 2011; Bourbousse et al. 2012; Nassrallah et al. 2018). However, it is not known whether Paf1C is present at many transcribed genes where it might contribute to H2Bub deposition or whether it affects this mark indifferently at all *loci*. To gain insight into transcription-associated chromatin mechanisms and their regulatory roles in plant development and stress responses, we examined the involvement of Paf1C in transcription elongation by RNAPII and in monoubiquitination of histone H2Bub throughout the Arabidopsis genome.

Results

The subunits of Paf1C ELF7 and VIP3 are recruited to gene bodies

First, we investigated the genomic distribution of Paf1C by profiling the chromatin association of the ELF7 and VIP3 subunits by Chromatin Immunoprecipitation Sequencing (ChIP-seq) in 1-wk-old Arabidopsis seedlings. ChIP-seq analyses were performed using the *pELF7:Flag-ELF7* and *35S:GFP-VIP3* transgenic lines (Dorcey et al. 2012; Cao et al. 2015), respectively, and nontransgenic WT plants as negative controls. The resulting analysis indicated a high correlation between biological replicates (Supplementary Fig. S1, A and B) and identified 9,791 and 6,845 Flag-ELF7 and GFP-VIP3 peaks, respectively (Fig. 1, A and B; Supplementary Tables S1 and S2), typically showing 1 peak per protein-coding gene (see examples in Supplementary Fig. S1C). Although the use of different promoters in the transgenic lines may lead to different levels and cellular accumulation patterns of FLAG-ELF7 and GFP-VIP3, the vast majority of peaks (6,057) were common, with 88% of GFP-VIP3 peaks matching FLAG-ELF7 peaks (Fig. 1A). A heatmap representation of Flag-ELF7 and GFP-VIP3 ChIP signal over unique and shared targeted genes confirmed that most of them were in fact bound by both proteins, albeit with different intensities (Supplementary Fig. S2A). Thus, for the next analyses, we considered all the peaks identified for the 2 subunits as bona fide Paf1C target loci (10,579) (Fig. 1A).

The genomic profile of Paf1C showed the strongest enrichment over gene bodies that slightly extend in 3′ over the transcription end site (TES) (Fig. 1, B to D; Supplementary Fig. S2A). Considering the proposed role of Paf1C in transcription elongation, we conducted a comparison with RNAPII profiles from wild-type seedlings obtained by ChIP-seq of the NRPB1 subunit, which indiscriminately captures all active RNAPII states (Supplementary Table S3). The analysis revealed that the overlap of the distributions of Paf1C and RNAPII was confined to gene bodies (Fig. 1B). The ELF7 distribution observed in this work was very similar to that found in 2 recent studies (see
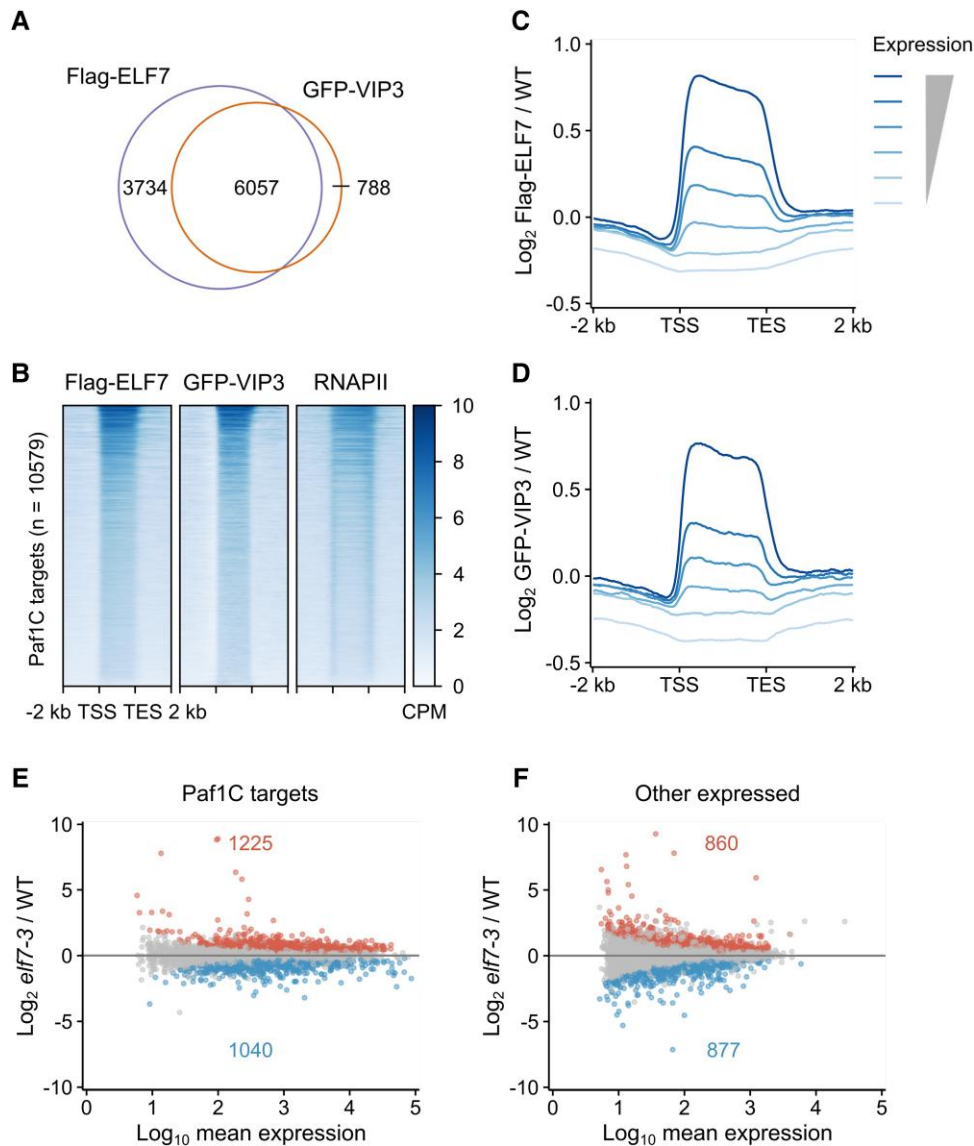
Figure 1. ELF7 and VIP3 bind to the gene body of transcribed genes. **A)** Venn diagram showing the overlap between Flag-ELF7 and GFP-VIP3 peaks. **B)** The heatmap shows the occupancy of Flag-ELF7, GFP-VIP3, and total RNAPII ranked by the decreasing Flag-ELF7 level. **C, D)** Average occupancy of Flag-ELF7 **C)** and GFP-VIP3 **D)** on target genes ranked by their expression level. Color intensity scale in **D)** is as in **C)**. **E, F)** MA plot with DEGs ($P_{adj} < 0.05$) in the *elf7-3* mutant compared with wild type for Paf1C target genes **E)** and for genes in which we could not detect Paf1C **F)**. In **E)** and **F)**, red and blue dots indicate upregulated and downregulated DEGs, respectively. WT, wild type; TSS, transcription start site; TES, transcription end site; CPM, counts per million mapped reads.

a comparison with the distribution found by Wang et al. in Supplementary Fig. S2B) (Obermeyer, Schrettenbrunner, et al. 2023; Wang, Zhong, et al. 2023). In accordance with Paf1C's role in transcription elongation, the occupancy of ELF7 and VIP3 exhibited a positive association with RNAPII occupancy (Fig. 1B) and transcript levels (Fig. 1, C and D). To further substantiate this perspective, we examined the accumulation of different histone marks and histone variants at Paf1C target genes (Jamge et al. 2023). Paf1C target genes were enriched in histone marks associated with active gene transcription, such as H3K4me3 and H3K36me3, while being depleted of the *Polycomb*-based H3K27me3 mark

(Supplementary Fig. S2A). Also consistent with Paf1C being associated with expressed genes and not with *Polycomb*-repressed genes, histone variant H2A.Z was enriched at the 5′ end but mostly absent across the gene bodies of Paf1C targets (Supplementary Fig. S2A) (Coleman-Derr and Zilberman 2012; Gómez-Zambrano et al. 2019).

To investigate the impact of Paf1C depletion on gene expression, we determined the transcriptome in wild-type and *elf7-3* 1-wk-old seedlings by RNA-seq. We identified 4,002 differentially expressed genes (DEGs; $P_{adj} < 0.05$) in *elf7-3* seedlings (Fig. 1, E and F; Supplementary Table S4). More than half of the identified DEGs (2,265) were bona fide Paf1C

targets (Fig. 1E; Supplementary Fig. S2C). Interestingly, when we plotted the average signal of Flag-ELF7 or GFP-VIP3 across DEGs in the "other expressed" category (Fig. 1F), corresponding to genes with no detectable Paf1C association, we found enrichment in gene bodies for both subunits compared with gene bodies of nonexpressed genes, consistent with the RNAPII signal (Supplementary Fig. S2C). This result suggests that the DEGs of the "other expressed" category are also target genes of Paf1C, although they are only weakly bound by the complex in accordance with their low expression level. The weak binding may be the reason that these genes were below the threshold to be detected by peak calling as true Paf1C targets. In any case, the DEGs represent a fraction of all loci bound to Paf1C in the genome, a situation similar to that observed in human cells knocked down for the ortholog Paf1 subunit (Yu et al. 2015). Among the bona fide Paf1C target DEGs, 1,040 were downregulated, consistent with a positive role of the complex on transcription elongation. Intriguingly, 1,225 DEGs were upregulated in the mutant, suggesting a negative impact of Paf1C on their expression or the existence of indirect effects mediating their induction in the absence of Paf1C.

Defects in the Paf1C complex affect the H2Bub mark genome wide

Paf1C is required for efficient monoubiquitination of H2B in various organisms, including plants (Wood et al. 2003; Schmitz et al. 2009; Hou et al. 2019; Li et al. 2023). To determine whether reduction of H2Bub deposition is detected at specific genes or on a global scale along the genome upon Paf1C loss of function, we examined the H2Bub dependence in wild-type and elf7-3 seedlings by ChIP-seq with spike-in of exogenous chromatin (ChIP-Rx). Following the protocol described in Nassrallah et al. (2018) for *Arabidopsis*, spike-in-based normalization enables accurate quantitative comparisons of samples with genome-wide differences in chromatin mark abundances. In our analyses, H2Bub was exclusively enriched in the transcribed regions (Fig. 2, A and B; Supplementary Table S5), in agreement with previous reports in *Arabidopsis* (Roudier et al. 2011; Bourbousse et al. 2012; Nassrallah et al. 2018). In addition, H2Bub-occupied genes were also co-occupied by Paf1C and RNAPII (Supplementary Fig. S3A), as expected for a cotranscriptionally deposited mark.

In the absence of Paf1C, H2Bub levels were strongly affected at multiple genes (Fig. 2, A and B; Supplementary Fig. S3, B and C). More precisely, the identification of differentially ubiquitinated genes showed a general tendency for reduced H2Bub enrichment over most H2Bub-marked genes in elf7-3 seedlings (Fig. 2C; Supplementary Table S6). Hence, given the frequent local co-occurrence of Flag-ELF7/GFP-VIP3 and the H2Bub mark, these observations suggest the existence of direct functional links between Paf1c activity and histone H2B monoubiquitination.

However, the association of Flag-ELF7 and GFP-VIP3 with chromatin was also found in genes enriched in RNAPII but not H2Bub (Fig. 2B; Supplementary Fig. S3C). We found
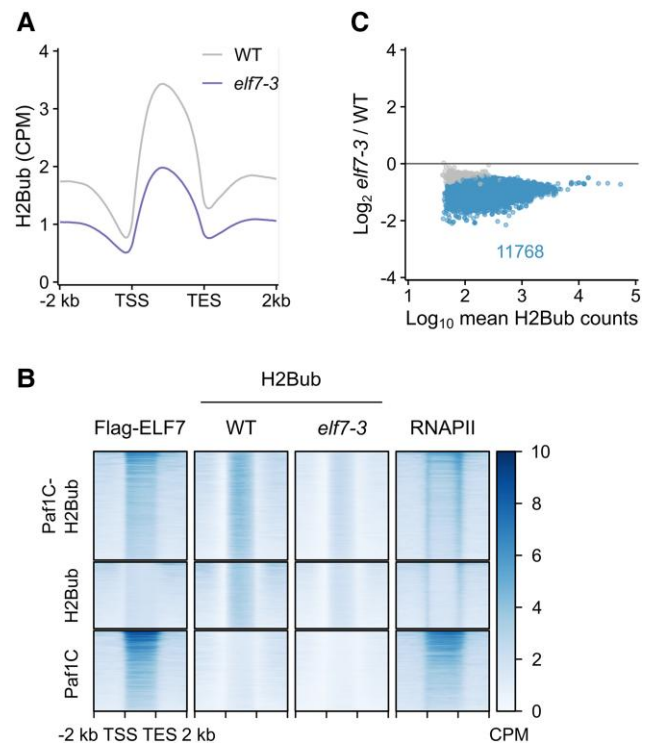
Figure 2. The H2Bub mark is reduced in elf7-3 mutants. **A)** Average occupancy of the H2Bub mark in the wild type and in the elf7-3 mutant. **B)** Heatmaps showing Flag-ELF7, H2Bub in wild-type and elf7-3 seedlings, and RNAPII occupancy in gene clusters based on H2Bub and Paf1C, H2Bub, or Paf1C occupancy. Genes are ranked by their decreasing levels of H2Bub in wild type. **C)** The MA plot shows differentially ubiquitinated genes (blue dots; $P_{adj} < 0.05$) between the wild-type and the elf7-3 mutant. WT, wild type; TSS, transcription start site; TES, transcription end site; CPM, counts per million mapped reads.

that these genes were smaller than those co-occupied by Paf1C and H2Bub (Supplementary Fig. S3D). As previously identified using transcriptome data (Bourbousse et al. 2012), this observation suggests that the optimal transcription of small genes in *Arabidopsis* is less dependent on H2Bub. Furthermore, it indicates that Paf1C may function independently of H2Bub deposition at multiple genes or that it may occupy these genes more persistently than H2Bub. Vice versa, H2Bub enrichment was detected at genes in which we could not detect Paf1C (Fig. 2B). Interestingly, H2Bub was also reduced at these genes in elf7-3 seedlings, possibly indicating that Paf1C acted on histone H2B monoubiquitination transiently, or earlier, at these loci. In summary, these observations suggest that histone H2B monoubiquitination is tightly linked to Paf1C activity at many genes but may also reflect the dynamic nature of Paf1C association to chromatin and H2Bub turnover during transcription. However, we cannot exclude that the lack of a complete association between the presence of Paf1C and the H2Bub mark observed in some of these genes may be due to technical limitations linked to stringent peak calling for detecting them or to Paf1C-independent H2Bub dynamics.

The H2Bub mark preferentially accumulates in longer genes in *Arabidopsis* (Supplementary Fig. S3D) (Roudier et al. 2011). On this basis, we decided to determine whether the requirement of Paf1C for histone H2B monoubiquitination is affected by gene size in plants. We ranked the H2Bub- and Paf1C-marked genes by gene size and compared the H2Bub signal in wild-type and *elf7-3* seedlings. This showed that the impact of Paf1C on H2Bub level is independent of gene size in *Arabidopsis* (Supplementary Fig. S4).

Studies in yeast and mammals provided molecular insights into the functional relationship between Paf1C and histone H2B monoubiquitination by the E2 conjugating enzyme Rad6 and the E3 ligase Bre1 in yeast and RNF20/RNF40 in mammals. In yeast, Paf1C promotes monoubiquitination through direct interaction with Rad6/Bre1 and does not appear to affect Rad6 recruitment to chromatin (Ng et al. 2003; Wood et al. 2003; Kim and Roeder 2009), whereas, in mammals, RNF20/40 recruitment to chromatin is dependent on Paf1C (Wu et al. 2014). To investigate the situation in *Arabidopsis*, we examined whether the reduction in the H2Bub mark in the *elf7-3* mutant was due to impaired recruitment to chromatin of HISTONE MONOUBIQUITINATION1 (HUB1) and HUB2, the 2 E3 ubiquitin ligases mediating H2Bub deposition in *Arabidopsis* (Liu et al. 2007). To this end, we fractionated cell extracts of the wild type and the *elf7-3* mutant and used a custom-made antibody to determine HUB1/2 levels (Fig. 3A) and their association with chromatin compared with cytoplasmic and nucleoplasmic fractions by immunoblotting. We observed a band corresponding to HUB1/2 in the chromatin fraction of wild-type cell extracts, and these levels were not affected by the *elf7-3* mutation (Fig. 3B; Supplementary Fig. S5). This result suggests that Paf1C promotes histone H2B monoubiquitination independently of HUB1/2 recruitment to chromatin in *Arabidopsis*.

Paf1C and histone H2B monoubiquitination regulate common processes

The functional relationship between Paf1C and H2Bub should manifest itself in common DEGs in mutants defective for Paf1C or for the machinery that monoubiquitinates histone H2B. We compared the transcriptomes of *elf7-3* and *hub1-4* mutant (Liu et al. 2007) seedlings grown side by side. We identified 413 DEGs ($P_{adj} < 0.05$) in *hub1-4* seedlings (Supplementary Table S7), a reduced number compared with *elf7-3* (Fig. 4, A and B). More than half of DEGs in *hub1-4* were also misregulated in *elf7-3* seedlings (Fig. 4B), and, importantly, this subset showed the same trend in gene expression change, in line with the functional link between Paf1C and H2Bub (Fig. 4, C and D). The majority of DEGs common to both mutants (170 out of 233) were occupied by Paf1C (Supplementary Fig. S6), suggesting direct functional links between Paf1C and H2Bub in gene expression.

Elf7 mutation causes RNAPII stalling at the 5′ end of genes

We next examined the effect of impaired Paf1C on RNAPII occupancy. ChIP-seq profiling of the NRPB1 subunit, which indiscriminately captures all active RNAPII states, detected peaks at 18,339 genes, half of which were also occupied by Paf1C. In wild-type plants, RNAPII distribution showed a typical pattern with peaks immediately after the transcription start site (TSS) and at the TES and lower levels throughout the gene body, which may be attributed to the high elongation rate and the shorter time spent by the RNAPII at that location (Figs. 1B, 2B, and 5A). The peak after the TSS reflected RNAPII stalled at the +1 nucleosome (Fig. 5B), as previously reported (Kindgren et al. 2019). Importantly, we observed a redistribution of RNAPII signal in the *elf7-3* mutant compared with wild-type plants, with reduced accumulation over gene bodies and TES and increased accumulation across the TSS region (Fig. 5, A and C). Overall, these defects most likely reflect a more frequent stalling of RNAPII in *elf7-3* plants.

Several lines of evidence pointed to a direct contribution of Paf1C to RNAPII redistribution. Reduction of RNAPII occupancy at gene bodies and TES in *elf7-3* seedlings was observed preferentially for Paf1C target genes (Fig. 5C). This suggests that Paf1C contributes locally to transcription elongation. Indeed, Paf1C target genes were enriched in histone marks associated with active transcription (Fig. 5C; Supplementary Fig. S2A). However, the increased accumulation of RNAPII at TSS observed in *elf7-3* seedlings also occurred in genes where no
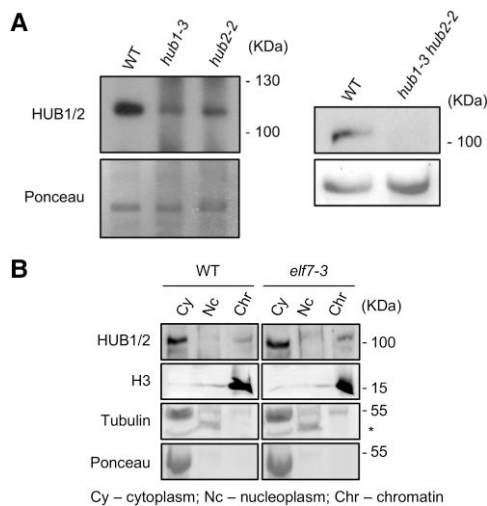
Figure 3. The recruitment of HUB1 and HUB2 to chromatin is independent of Paf1C. **A)** Immunoblot showing that the antiserum detects both HUB1 and HUB2. Although the antiserum was raised against a HUB1-specific peptide, it recognizes both HUB1 and HUB2 proteins, most likely because the antibody recognizes the secondary structure of the peptide rather than its sequence. The bottom panels show the Ponceau staining. **B)** Detection of HUB1/HUB2 in cytoplasmic, nucleoplasmic, and chromatin fractions by Western blot analysis. Histone H3 was used as a chromatin marker and tubulin and Ponceau staining as cytoplasmic markers. The position of the molecular weight markers is shown on the right. The asterisk marks a nonspecific band detected with the anti-tubulin antibody. WT, wild type.
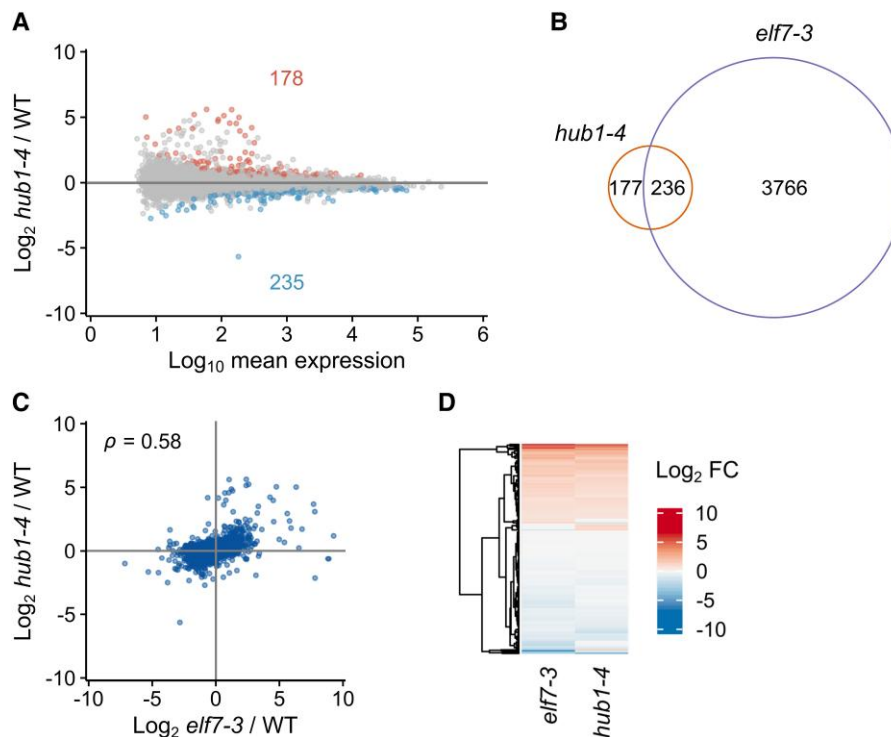
Figure 4. HUB1 and ELF7 regulate a common set of genes. **A)** MA plot showing DEGs ($P_{adj} < 0.05$) between *hub1-4* and wild-type seedlings. Red and blue dots indicate upregulated and downregulated DEGs, respectively. **B)** Comparison of DEGs between *hub1-4* and *elf7-3* seedlings. **C)** Scatter plot showing the correlation of common DEGs between *hub1-4* and *elf7-3* mutant seedlings. **D)** The heatmap shows the behavior of common DEGs between *hub1-4* and *elf7-3* mutant seedlings. WT, wild type.

Paf1C peak was detected (Fig. 5C). This result suggests that the effect of the *elf7-3* mutation on stalled RNAPII may result from direct and indirect consequences of defective Paf1C, such as reduced H2B monoubiquitination (Fig. 5C). Interestingly, the accumulation of stalled RNAPII in *elf7-3* mutant plants was shifted toward the 5′ end of the genes compared with wild type (Fig. 5B). However, it is unclear whether this shift is due to the +1 nucleosome moving toward the 5′ end of the genes in the mutant.

Finally, the possibility that Paf1C is involved in transcription elongation was further supported by comparing the RNAPII pausing index of wild-type and *elf7-3* mutant plants. Similar to previous studies (Wang, Fan, et al. 2023), we calculated the pausing index as the ratio of RNAPII occupancy across the TSS to RNAPII occupancy in the gene body (Fig. 5D). As shown in Fig. 5E, the RNAPII pausing index increased in plants of the Paf1C mutant. This is consistent with the idea that Paf1C contributes to the productive elongation of RNAPII.

Discussion

In this study, we provide genome-wide evidence for the function of Paf1C as a transcriptional elongation factor in plants. First, the Paf1C subunits ELF7 and VIP3 are exclusively distributed in gene bodies, and their accumulation positively associates with that of RNAPII and gene expression, suggesting that

the complex actively promotes gene transcription (Fig. 1, B to D; Supplementary Fig. S2). Second, monoubiquitination of histone H2B, a chromatin mark that is deposited cotranscriptionally, is severely reduced in virtually all genes in Paf1C-defective plants, a defect that is particularly pronounced in Paf1C-targeted genes (Figs. 2 and 4C). Third, RNAPII appears to stall more frequently at the 5′ end of genes, and the overall gene body occupancy is reduced in Paf1C-targeted genes in *elf7-3* mutant plants (Fig. 4, A to C). This likely reflects the inability of RNAPII to transition to the productive elongation stage. The latter is consistent with previous results in *Arabidopsis*, which demonstrate that (i) the phosphorylated form of RNAPII at serine 5 (Ser5) of the C-terminal domain of NRPB1 (RNAPII-Ser5), marking engaged RNAPII, accumulates in the *elf7-3* mutant around the TSS (Wang, Zhong, et al. 2023); (ii) the occupancy at gene bodies of Ser2 phosphorylated RNAPII, the elongating form, is reduced in the *elf7-3* mutant (Obermeyer et al. 2022); and (iii) the reads of the newly synthesized RNA accumulate toward the TSS and are reduced in the gene body in *elf7-3* seedlings compared with the wild type (Obermeyer, Schrettenbrunner, et al. 2023).

Despite this evidence for a role of Paf1C in transcription elongation, we still lack information on the mechanism of action of this complex in plants. In this regard, a comparison of the genomic distribution of Paf1C and RNAPII in different model organisms could provide relevant information. The
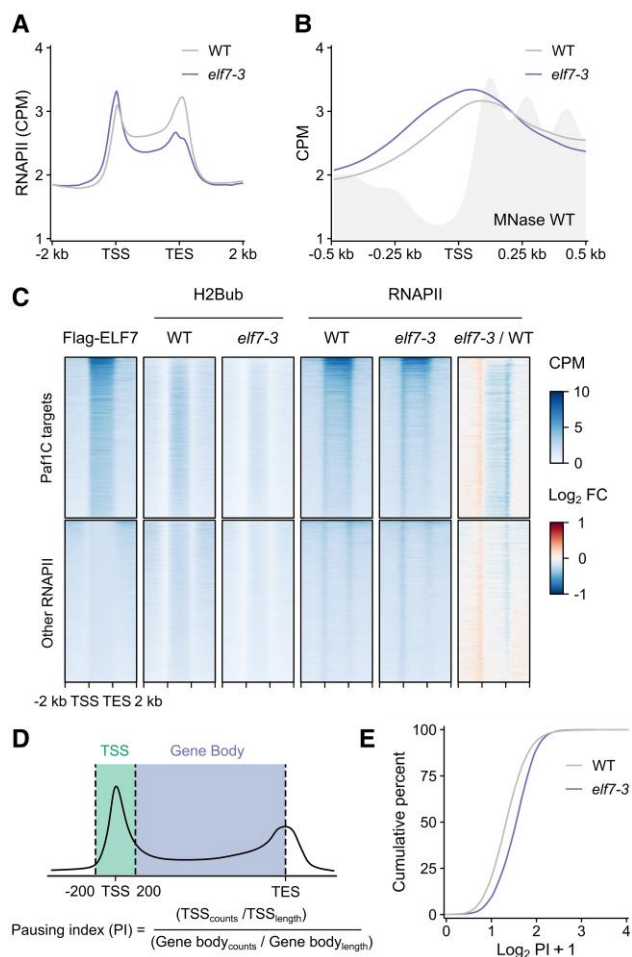
Figure 5. RNAPII genomic distribution is affected in *elf7-3* seedlings. **A)** The metagene analysis shows the average distribution of all RNAPII-occupied genes in wild-type and in *elf7-3* mutants. **B)** Average distributions of RNAPII in wild-type and *elf7-3* seedlings centered on the TSS and compared with the nucleosome position previously determined by MNase-seq (Diego-Martín et al. 2022). **C)** The heatmap shows the effect of the *elf7-3* mutation on the distribution of RNAPII and H2Bub in genes occupied by Paf1C (Paf1C targets) and in genes in which we could not detect binding of Paf1C (other RNAPII). The Log$_2$ fold change (FC) scale specifically pertains to the *elf7*/WT heatmap, while CPM scale is applicable to all others. **D)** Scheme depicting the calculation used to determine the pausing index (PI). **E)** Representation of the PI in wild-type and *elf7-3* mutant. The higher the PI, the greater the degree of paused RNAPII. WT, wild type; TSS, transcription start site; TES, transcription end site; CPM, counts per million mapped reads.

genomic profile of the *Arabidopsis* Paf1C subunits ELF7 and VIP3 strongly resembles that of the Paf1 subunit in yeast, as both are mainly localized within the gene bodies (Fig. 1, B and C) (Mayer et al. 2010; Wang, Zhong, et al. 2023). It is noteworthy, however, that while RNAPII, much like Paf1C, is found within gene bodies, their distributions do not entirely overlap, as RNAPII exhibits heightened enrichment at the TSS and TES (Figs. 1B and 5B). In mammals, the distribution of Paf1C parallels the distribution of RNAPII, as both are

enriched across the TSS and after the TES (Rahl et al. 2010; Chen et al. 2015; Yu et al. 2015). In mammals, their similar distributions, therefore, reflect an association of Paf1C with RNAPII, with Paf1C involved in the regulation of RNAPII pausing immediately after the TSS (Chen et al. 2015; Yu et al. 2015) and contributing to mRNA polyadenylation (Nagaike et al. 2011). However, in *Arabidopsis*, the genes are generally much shorter than in mammals. Consistent with the positive association observed in mammals between the distribution of Paf1C and RNAPII, the accumulation of Paf1C at gene bodies in *Arabidopsis* may be important for productive transcription elongation, as shown in Fig. 5C. Consistent with this possibility, RNAPII accumulates near the TSS of genes and is locally shifted toward 5′, whereas the RNAPII pausing index is increased in the *elf7* mutant compared with wild-type plants.

How does Paf1C contribute to transcriptional elongation? The association of Paf1C with RNAPII could facilitate the passage of the transcriptional machinery through the nucleosomes through several mechanisms. Structural studies in mammals have shown that Paf1C position in the RNAPII transcriptional complex should enable it to promote methylation of histone H3K4 in downstream nucleosomes—a modification known to facilitate transcription (Vos et al. 2018). We hypothesize that Paf1C would be recruited to RNAPII, positioning itself within the complex similarly to its mammalian counterpart. Subsequently, Paf1C would promote posttranslational modifications of histones, such as monoubiquitination of H2B in nucleosomes downstream of the +1, thereby facilitating the passage of RNAPII throughout the whole gene body where we found both Paf1C and H2Bub to accumulate frequently. The direct effect of Paf1C on local HUB1/2 activity is supported by several observations in this study, including the frequent co-occupancy of genes by Paf1C and RNAPII, with high levels of H2Bub in this context, the association of HUB1/2 with chromatin even in the absence of Paf1C, and the previously described physical interaction between the Paf1C subunit VIP5 and the *Arabidopsis* homologs of the Rad6 E2 ubiquitin-conjugating enzyme (Li et al. 2023). Nevertheless, the reduced H2Bub deposition in *elf7* mutant plants could, in some cases, result from indirect effects of Paf1C deficiency, such as impaired RNAPII elongation.

Materials and methods

Plant material
The *Arabidopsis* (*A. thaliana*) lines used in this work have been previously described: *elf7-3* (He et al. 2004), *hub1-4* and *hub1-3 hub2-2* (Liu et al. 2007), *pELF7:Flag-ELF7 elf7-3* (Cao et al. 2015), and *35S:GFP-VIP3* (Dorcey et al. 2012).

Growth conditions and treatments
All seeds were surface sterilized and sown on half-strength MS (Duchefa) plates containing 1% (*w/v*) sucrose and 8-g/L agar (pH 5.7). Seedlings were grown at 22 °C under continuous light (50 to 60 μmol m^{-2} s^{-1}) (standard conditions).

RNA-seq experiments

RNA-seq with 3 independent biological replicates for each genotype was performed. Seedlings were grown as described above. Seven-day-old wild-type, *elf7-3*, and *hub1-4* seedlings were collected. Total RNA was extracted using an RNeasy Plant Mini Kit (Qiagen) according to the manufacturer's instructions. RNA concentration and integrity were measured in an RNA Nanochip (Bioanalyzer, Agilent Technologies 2100) from IBMCP Genomics Service. Library preparation and sequencing were performed by the Genomics Service of the University of Valencia.

RNA-seq analysis

RNA-seq read quality was first evaluated using FastQC v0.11.9. Low-quality bases and Illumina adapters were trimmed using cutadapt v4.2 with options "-q 15,10 -a AGATCGGAAGAG CACACGTCTGAACTCCAGTCA -m 20 --trim-n". Clean reads were then aligned to the TAIR10 reference genome using STAR v2.7.10b ([Dobin et al. 2013](#)) with the default parameters. Read counts were obtained using the feature Counts command from subread v2.0.3 ([Liao et al. 2014](#)) with the default parameters and providing the Araport11 annotation ([Supplementary Table S8](#)). Differential analyses were performed using DESeq2 v1.38 ([Love et al. 2014](#)). Genes showing an adjusted P-value inferior to 0.05 were considered as differentially expressed.

ChIP experiments

H2B and H2Bub ChIP-Rx were performed in parallel with the same 2 biological replicates of 7-d-old wild-type and *elf7-3* seedlings grown under standard conditions. As previously described ([Nassrallah et al. 2018](#)), all samples were spiked in with *Drosophila* chromatin prior to IP. The amount of exogenous DNA was subsequently determined in all input and IP samples and considered as a reference to avoid the effects of technical variation. Furthermore, we determined the H2Bub peaks after normalization to histone H2B occupancy determined in the same samples by ChIP-Rx. Specifically, for each biological replicate, 2 IPs were performed with an anti-H2Bub antibody (MM -0029-P, Medimabs) and 1 IP with an anti-H2B (ab1790, Abcam). For each IP, 100 μg of *Arabidopsis* chromatin mixed with 3 μg of *Drosophila* chromatin was used. DNA eluted from the 2 technical replicates of the H2Bub IP was pooled prior to library preparation. Library preparation and sequencing were performed by the CRG Genomics Core Facility (Barcelona, Spain). Flag-ELF7 and GFP-VIP3 ChIP-seqs were performed using 2 biological replicates of 7-d-old seedlings grown under standard conditions and an anti-Flag M2 antibody (F1804, Sigma) and an anti-GFP antibody (ab290, Abcam), respectively. We used double in vitro cross-linking with 1.5 mM ethylene glycol bis (succinimidyl succinate) for 20 min, followed by 1% formaldehyde for 10 min at room temperature. Library preparation and sequencing were performed by the CRG Genomics Core Facility (Barcelona, Spain). ChIP-seq for RNAPII was performed using an anti-RPB1 antibody (clone 4H8, Active Motif) using 2 biological replicates of 7-d-old wild-type and *elf7-3* seedlings grown under standard conditions. Library preparation and sequencing were performed by the epigenomic platform at IPS2 (Paris, France).

ChIP-seq analysis

The quality of ChIP-seq reads was first assessed using FastQC v0.11.9. Low-quality bases and Illumina adapters were trimmed using cutadapt v4.2 with options "-q 15,10 -a AGATCGGAAGA GCACACGTCTGAACTCCAGTCA -m 20". Clean reads were then aligned to the TAIR10 reference genome using bowtie2 v2.5.1 ([Langmead and Salzberg 2012](#)) with the default parameters. Alignments were sorted by coordinate using the SAMtools sort command from SAMtools v1.17 ([Li et al. 2009](#)). Duplicate reads were then marked using the sambamba markdup command from sambamba v1.0 ([Tarasov et al. 2015](#)), and uniquely mapped reads were retained using the SAMtools view command with options "-F 4 -F 1024 -q 5" ([Supplementary Table S8](#)). Coverage files in bedGraph format were obtained using the genomeCoverageBed command from BEDTools v2.31.0 ([Quinlan 2014](#)) with options "-bga -fs 200", and then, these were converted to bigwig using the bedGraphToBigWig command. Bigwigs were normalized to counts per million (CPM) using the WiggleTools scale command from WiggleTools v1.2 ([Zerbino et al. 2014](#)). Mean coverages of biological replicates from each condition were obtained using the WiggleTools mean command. Log2 ratios between treatments, and controls were obtained using the bigwigCompare command from deepTools v3.5.1 ([Ramírez et al. 2014](#)).

Peak calling was performed over uniquely mapped reads using macs2 callpeak from macs2 v2.2.7.1 ([Zhang et al. 2008](#)) with the following parameters: "--keep-dup all --broad --broad-cutoff 0.05 -q 0.01 --nomodel --extsize 200". Peaks from biological replicates were pooled and merged into a consensus set using the BEDTools merge command from BEDTools v2.31.0 ([Quinlan 2014](#)). In experiments that included various treatments (ChIP-seq of H2Bub and RNAPII), the consensus peaks were obtained by merging the peaks from each treatment using the same procedure as for the biological replicates. Consensus peaks were annotated to their closest gene using the BEDTools closest command. To determine which genes could be considered as targets, the following filters were applied: the peak must overlap more than half of the gene body, or the gene body must overlap more than half of the peak, or the peak center must be less than 200 pb away from the TSS.

ChIP-Rx analysis

H2Bub ChIP-Rx reads were first processed the same way as ChIP-seq reads. Clean reads were aligned against a chimeric genome that contained both *Arabidopsis* (TAIR10) and *Drosophila melanogaster* (dm6) chromosomes ([Supplementary Table S9](#)). Alignments were sorted and duplicate marked as in ChIP-seq, and then, reads that mapped to TAIR10 or to dm6 were separated. TAIR10 alignments

were filtered and used to create coverage bigwigs and for peak calling as previously described. Rx normalization factors were calculated as described in Nassrallah et al. (2018). Briefly, the normalization factor α for each ChIP sample was obtained using the following formula:

$$\alpha = \frac{r}{N_d \text{IP}},$$

where N_d is the number of mapped reads to *Drosophila* dm6 in millions, and r is the percentage of dm6 reads in the corresponding input sample. Hence, r was calculated as:

$$r = \frac{N_d i}{(N_d i + N_a i)} \times 100,$$

where $N_d i$ and $N_a i$ are the number of reads mapped to dm6 and TAIR10.

To test differential ubiquitination, read counts over the consensus H2Bub peaks were first obtained using the multiBamSummay command from deepTools v3.5.1 (Ramírez et al. 2014) with options "--extendReads 200 --minMappingQuality 5". Gene level counts were obtained by summing counts from peaks that were annotated to the same gene. Differential analyses were performed using DESeq2 v1.38.0 (Love et al. 2014). In these analyses, the Rx normalization factors were provided as size factors. Genes showing an adjusted *P*-value inferior to 0.05 were considered as differentially ubiquitinated.

Pausing index
To estimate RNAPII pausing, the pausing index formula was employed (Wang, Fan, et al. 2023):

$$\text{PI} = \frac{\text{TSS}_{\text{counts}}/\text{TSS}_{\text{length}}}{\text{GeneBody}_{\text{counts}}/\text{GeneBody}_{\text{length}}}.$$

The TSS was defined as a 400-bp region centered in the annotated TSS, whereas the gene body spanned from the TSS region to the annotated TES. For this reason, only RNAPII genes that were longer than 200 pb were included. BEDfiles of TSSs and gene bodies were created using the slopBed command from BEDTools v2.31.0 (Quinlan 2014) and the TAIR10 reference annotation. Counts over these regions were then obtained using the multiBamSummary command from deepTools v3.5.1 (Ramírez et al. 2014).

Reanalysis of existing datasets
ChIP-seq reads of H3, H3K4me3, H3K36me3, H3K27me3, and H2A.Z (GSE231408: samples GSM7075958, GSM7075959, GSM7075961, GSM7075962, GSM7075963, GSM7075964, GSM7075985, GSM7075986, and GSM7075990) (Jamge et al. 2023) were analyzed as described in ChIP-seq analysis. MNase-seq reads of wild-type Col-0 (GSE205110: samples GSM6205325 and GSM6205326) (Diego-Martín et al. 2022)

were downloaded, processed, and aligned as described in ChIP-seq analysis. Coverage bigwigs were obtained using DANPOS v2.2.2 (Chen et al. 2013) and the wigToBigWig command.

Data representations
Graphs were plotted in R 4.1.2 using ggplot2, eulerr, and ComplexHeatmap libraries (Gu et al. 2016). Other heatmaps and metaplots were obtained using the computeMatrix, plotHeatmap, and plotProfile commands from deepTools v3.5 (Ramírez et al. 2014).

Subcellular fractionation
Cytoplasmic, nucleoplasmic, and chromatin-associated fractions were obtained following a described protocol (Liu et al. 2018), with some minor modifications. Briefly, approximately 1.5 g of 7-d-old seedlings were ground in liquid nitrogen and subsequently homogenized in 3 to 4 mL of Honda buffer (0.44 M sucrose, 20 mM HEPES KOH pH 7.4, 2.5% [v/v] Percoll, 5% [w/v] Dextran T40, 10 mM MgCl$_2$, 0.5% [v/v] Triton X-100, 5 mM DTT, 1 mM PMSF, and 1× protease inhibitor cocktail [cOmplete, EDTA-free; Roche]). The resulting homogenate was filtered through 2 layers of Miracloth, and the flow through was then subjected to centrifugation at 2,400 × g for 10 min at 4 °C. The resulting supernatant (1 mL) was further centrifuged at 10,000 × g for 10 min at 4 °C, and this supernatant was collected as the cytoplasmic fraction. The pellet was resuspended in 1 mL of Honda buffer and centrifuged at 1,800 × g for 5 min at 4 °C to concentrate nuclei. This pellet was subsequently washed 4 to 6 times with Honda buffer and rinsed with PBS buffer (137 mM NaCl, 2.7 mM KCl, 10 mM Na$_2$HPO$_4$, and 2 mM KH$_2$PO$_4$) containing 1 mM EDTA. The resulting pellet was resuspended in 150 μL of cold glycerol buffer (20 mM Tris–HCl pH 7.9, 50% [v/v] glycerol, 75 mM NaCl, 0.5 mM EDTA, 0.85 mM DTT, 0.125 mM PMSF, and 1× protease inhibitor cocktail [cOmplete, EDTA-free; Roche]) and gently vortexed twice after adding 150 μL of cold nuclei lysis buffer (10 mM HEPES KOH pH 7.4, 7.5 mM MgCl$_2$, 0.2 mM EDTA, 0.3 M NaCl, 1 M urea, 1% [v/v] NP-40, 1 mM DTT, 0.5 mM PMSF, 10 mM β-mercaptoethanol, and 1× protease inhibitor cocktail [cOmplete, EDTA-free; Roche]). The mixture was then incubated for 2 min on ice and centrifuged at 10,000 × g for 2 min at 4 °C. The resulting supernatant was collected as the nucleoplasmic fraction. The chromatin-associated pellet was rinsed with PBS buffer containing 1 mM EDTA and then resuspended in 150 μL of cold glycerol buffer plus 150 μL of cold nuclei lysis buffer. Protein concentrations were determined using the Pierce 660 nm Protein Assay following the manufacturer's instructions. The various fractions were subsequently analyzed by immunoblot.

Immunoblot analysis
Total protein extracts and subcellular fractionation samples were separated with SDS–PAGE, transferred to PVDF membranes, and immunolabeled with commercial antibodies against histone H3 (ab1791, Abcam) and against tubulin

(62204, Invitrogen). Chemiluminescence was detected using the Supersignal west FEMTO substrate with maximum sensitivity (Thermo Fisher Scientific), and protein bands were detected and quantified using the LAS-3000 Imaging System (Fujifilm) and ImageJ software, respectively. The custom-made rabbit anti-HUB1 antibody was generated for F. Barneche by SDIX (Newark, USA) using the following immunogen sequence MQDTLLIDKYIMDKDIQQGSAYASF LSKKSSRIEDQLRFCTDQFQKLAEDKYQKSVSLENL QKKRADI GNGLEQARSRLEESHSKVEQSRLDYGALELEL.

Accession numbers

Sequence data from this article can be found in the Arabidopsis Genome Initiative under the following accession numbers: ELF7 (AT1G79730), VIP3 (AT4G29830), HUB1 (AT2G44950), and HUB2 (AT1G55250). The sequencing data generated in this work have been deposited in the GEO public functional genomics data repository under the accession number GSE244850.

Acknowledgments

Author contributions

N.B.-T., J.P.-A., C.B., M.B., F.B., M.A.B., J.G.-B., and D.A. designed the research; N.B.-T., J.P.-A., C.B., D.L., O.A., M.B., F.B., J.G.-B., and D.A. performed research; N.B.-T., J.P.-A., C.B., D.L., O.A., M.B., F.B., M.A.B., J.G.-B., and D.A. analyzed data; and D.A. wrote the paper.

Supplementary data

The following materials are available in the online version of this article.

Supplementary Figure S1. The Paf1C subunits ELF7 and VIP3 bind to common targets.

Supplementary Figure S2. Binding of ELF7 and VIP3 associates with epigenetic marks linked to active gene expression.

Supplementary Figure S3. Dependent and independent effects of Paf1C on H2Bub marking.

Supplementary Figure S4. The effect of Paf1C on H2Bub is independent on gene size.

Supplementary Figure S5. The recruitment of HUB1 and HUB2 to chromatin is independent of Paf1C.

Supplementary Figure S6. Venn diagram showing the overlap between common DEGs of *hub1-4* and *elf7-3* mutants and Paf1C targets.

Supplementary Table S1. Annotated peaks from the FLAG-ELF7 ChIP-seq.

Supplementary Table S2. Annotated peaks from the GFP-VIP3 ChIP-seq.

Supplementary Table S3. Annotated peaks from the NRPB1 ChIP-seq.

Supplementary Table S4. Differential expression analysis of *elf7-3* compared with wild-type seedlings.

Supplementary Table S5. Annotated peaks from the H2Bub ChIP-Rx.

Supplementary Table S6. Differential H2B monoubiquitination analysis of *elf7-3* compared with wild-type seedlings.

Supplementary Table S7. Differential expression analysis of *hub1-4* compared with wild-type seedlings.

Supplementary Table S8. Number of total and filtered reads in ChIP-seq, ChIP-Rx, and RNA-seq experiments.

Supplementary Table S9. Number of reads mapped to the *D. melanogaster* genome in the ChIP-Rx experiment.

Funding

Data availability

The data underlying this article are available in the GEO public functional genomics data repository at www.ncbi.nlm.nih.gov/geo/ under the accession number GSE244850.

References

Antosz W, Pfab A, Ehrnsberger HF, Holzinger P, Köllen K, Mortensen SA, Bruckmann A, Schubert T, Längst G, Griesenbeck J, et al. The composition of the *Arabidopsis* RNA polymerase II transcript elongation complex reveals the interplay between elongation and mRNA processing factors. Plant Cell. 2017:**29**(4):854–870. https://doi.org/10.1105/tpc.16.00735

Bourbousse C, Ahmed I, Roudier F, Zabulon G, Blondet E, Balzergue S, Colot V, Bowler C, Barneche F. Histone H2B monoubiquitination facilitates the rapid modulation of gene expression during *Arabidopsis* photomorphogenesis. PLoS Genet. 2012:**8**(7):e1002825. https://doi.org/10.1371/journal.pgen.1002825

Cao Y, Wen L, Wang Z, Ma L. SKIP interacts with the Paf1 Complex to regulate flowering via the activation of FLC transcription in *Arabidopsis*. Mol Plant. 2015:**8**(12):1816–1819. https://doi.org/10.1016/j.molp.2015.09.004

Chen F, Woodfin A, Gardini A, Rickels R, Marshall S, Smith E, Shiekhattar R, Shilatifard A. PAF1, a molecular regulator of promoter-proximal pausing by RNA polymerase II. Cell. 2015:**162**(5):1003–1015. https://doi.org/10.1016/j.cell.2015.07.042

Chen K, Xi Y, Pan X, Li Z, Kaestner K, Tyler J, Dent S, He X, Li W. DANPOS: dynamic analysis of nucleosome position and occupancy by sequencing. Genome Res. 2013:**23**(2):341–351. https://doi.org/10.1101/gr.142067.112

Coleman-Derr D, Zilberman D. Deposition of histone variant H2A.Z within gene bodies regulates responsive genes. PLoS Genet. 2012:**8**(10):e1002988. https://doi.org/10.1371/journal.pgen.1002988

Diego-Martín B, Pérez-Alemany JP, Candela-Ferré J, Corbalán-Acedo A, Pereyra J, Alabadí D, Jami-Alahmadi Y, Wohlschlegel J, Gallego-Bartolomé J. The TRIPLE PHD FINGERS proteins are required for SWI/SNF complex-mediated +1 nucleosome positioning and transcription start site determination in *Arabidopsis*. Nucleic Acids Res. 2022:**50**(18):10399–10417. https://doi.org/10.1093/nar/gkac826

Dobin A, Davis CA, Schlesinger F, Drenkow J, Zaleski C, Jha S, Batut P, Chaisson M, Gingeras TR. STAR: ultrafast universal RNA-seq aligner. Bioinformatics. 2013:**29**(1):15–21. https://doi.org/10.1093/bioinformatics/bts635

Dorcey E, Rodriguez-Villalon A, Salinas P, Santuari L, Pradervand S, Harshman K, Hardtke CS. Context-dependent dual role of SKI8 homologs in mRNA synthesis and turnover. PLoS Genet. 2012:**8**(4):e1002652. https://doi.org/10.1371/journal.pgen.1002652

Fal K, Cortes M, Liu M, Collaudin S, Das P, Hamant O, Trehin C. Paf1c defects challenge the robustness of flower meristem termination in *Arabidopsis thaliana*. Development. 2019:**146**:dev173377. https://doi.org/10.1242/dev.173377

Fal K, Liu M, Duisembekova A, Refahi Y, Haswell ES, Hamant O. Phyllotactic regularity requires the paf1 complex in *Arabidopsis*. Development. 2017:**144**(23):4428–4436. https://doi.org/10.1242/dev.154369

Francette AM, Tripplehorn SA, Arndt KM. The Paf1 complex: a keystone of nuclear regulation operating at the interface of transcription and chromatin. J Mol Biol. 2021:**433**(14):166979. https://doi.org/10.1016/j.jmb.2021.166979

Gómez-Zambrano Á, Merini W, Calonje M. The repressive role of *Arabidopsis* H2A.Z in transcriptional regulation depends on AtBMI1 activity. Nat Commun. 2019:**10**(1):2828. https://doi.org/10.1038/s41467-019-10773-1

Gu Z, Eils R, Schlesner M. Complex heatmaps reveal patterns and correlations in multidimensional genomic data. Bioinformatics. 2016:**32**(18):2847–2849. https://doi.org/10.1093/bioinformatics/btw313

He Y, Doyle MR, Amasino RM. PAF1-complex-mediated histone methylation of FLOWERING LOCUS C chromatin is required for the vernalization-responsive, winter-annual habit in *Arabidopsis*. Genes Dev. 2004:**18**(22):2774–2784. https://doi.org/10.1101/gad.1244504

Hou L, Wang Y, Liu Y, Zhang N, Shamovsky I, Nudler E, Tian B, Dynlacht BD. Paf1C regulates RNA polymerase II progression by modulating elongation rate. Proc Natl Acad Sci U S A. 2019:**116**(29):14583–14592. https://doi.org/10.1073/pnas.1904324116

Jamge B, Lorković ZJ, Axelsson E, Osakabe A, Shukla V, Yelagandula R, Akimcheva S, Kuehn AL, Berger F, Biocenter V, et al. Histone variants shape chromatin states in *Arabidopsis*. eLife. 2023:**12**:RP87714. https://doi.org/10.7554/eLife.87714

Kim J, Roeder RG. Direct Bre1-Paf1 complex interactions and RING finger-independent Bre1-Rad6 interactions mediate histone H2B ubiquitylation in yeast. J Biol Chem. 2009:**284**(31):20582–20592. https://doi.org/10.1074/jbc.M109.017442

Kindgren P, Ivanov M, Marquardt S. Native elongation transcript sequencing reveals temperature dependent dynamics of nascent RNAPII transcription in *Arabidopsis*. Nucleic Acids Res. 2019:**48**(5):2332–2347. https://doi.org/10.1093/nar/gkz1189

Langmead B, Salzberg SL. Fast gapped-read alignment with Bowtie 2. Nat Methods. 2012:**9**(4):357–359. https://doi.org/10.1038/nmeth.1923

Li C, Guo Y, Wang L, Yan S. The SMC5/6 complex recruits the PAF1 complex to facilitate DNA double-strand break repair in *Arabidopsis*. EMBO J. 2023:**42**(7):e112756. https://doi.org/10.15252/embj.2022112756

Li H, Handsaker B, Wysoker A, Fennell T, Ruan J, Homer N, Marth G, Abecasis G, Durbin R. The sequence alignment/map format and SAMtools. Bioinformatics. 2009:**25**(16):2078–2079. https://doi.org/10.1093/bioinformatics/btp352

Li R, Wei Z, Li Y, Shang X, Cao Y, Duan L, Ma L. SKI-INTERACTING PROTEIN interacts with SHOOT MERISTEMLESS to regulate shoot apical meristem formation. Plant Physiol. 2022:**189**(4):2193–2209. https://doi.org/10.1093/plphys/kiac241

Li Y, Yang J, Shang X, Lv W, Xia C, Wang C, Feng J, Cao Y, He H, Li L, et al. SKIP regulates environmental fitness and floral transition by forming two distinct complexes in *Arabidopsis*. New Phytologist. 2019:**224**(1):321–335. https://doi.org/10.1111/nph.15990

Liao Y, Smyth GK, Shi W. FeatureCounts: an efficient general purpose program for assigning sequence reads to genomic features. Bioinformatics. 2014:**30**(7):923–930. https://doi.org/10.1093/bioinformatics/btt656

Liu C, Xin Y, Xu L, Cai Z, Xue Y, Liu Y, Xie D, Liu Y, Qi Y. *Arabidopsis* ARGONAUTE 1 binds chromatin to promote gene transcription in response to hormones and stresses. Dev Cell. 2018:**44**(3):348–361.e7. https://doi.org/10.1016/j.devcel.2017.12.002

Liu Y, Geyer R, van Zanten M, Carles A, Li Y, Hörold A, van Nocker S, Soppe WJ. Identification of the *Arabidopsis* REDUCED DORMANCY 2 gene uncovers a role for the polymerase associated factor 1 complex in seed dormancy. PLoS One. 2011:**6**(7):e22241. https://doi.org/10.1371/journal.pone.0022241

Liu Y, Koornneef M, Soppe WJ. The absence of histone H2B monoubiquitination in the *Arabidopsis* hub1 (rdo4) mutant reveals a role for chromatin remodeling in seed dormancy. Plant Cell. 2007:**19**(2):433–444. https://doi.org/10.1105/tpc.106.049221

Love MI, Huber W, Anders S. Moderated estimation of fold change and dispersion for RNA-seq data with DESeq2. Genome Biol. 2014:**15**(12):1–21. https://doi.org/10.1186/s13059-014-0550-8

Lu C, Tian Y, Wang S, Su Y, Mao T, Huang T, Chen Q, Xu Z, Ding Y. Phosphorylation of SPT5 by CDKD; 2 is required for VIP5 recruitment and normal flowering in *Arabidopsis thaliana*. Plant Cell. 2017:**29**(2):277–291. https://doi.org/10.1105/tpc.16.00568

Mayer A, Lidschreiber M, Siebert M, Leike K, Söding J, Cramer P. Uniform transitions of the general RNA polymerase II transcription complex. Nature Structural and Molecular Biology. 2010:**17**(10):1272–1278. https://doi.org/10.1038/nsmb.1903

Nagaike T, Logan C, Hotta I, Rozenblatt-Rosen O, Meyerson M, Manley JL. Transcriptional activators enhance polyadenylation of mRNA precursors. Mol Cell. 2011:**41**(4):409–418. https://doi.org/10.1016/j.molcel.2011.01.022

Nasim Z, Susila H, Jin S, Youn G, Ahn JH. Polymerase II–associated factor 1 complex-regulated FLOWERING LOCUS C-clade genes repress flowering in response to chilling. Front Plant Sci. 2022:**13**:817356. https://doi.org/10.3389/fpls.2022.817356

Nassrallah A, Rougée M, Bourbousse C, Drevensek S, Fonseca S, Iniesto E, Ait-Mohamed O, Deton-Cabanillas AF, Zabulon G, Ahmed I, et al. DET1-mediated degradation of a SAGA-like deubiquitination module controls H2Bub homeostasis. eLife. 2018:**7**:e37892. https://doi.org/10.7554/eLife.37892

Ng HH, Dole S, Struhl K. The Rtf1 component of the Paf1 transcriptional elongation complex is required for ubiquitination of histone H2B. Journal of Biological Chemistry. 2003:**278**(36):33625–33628. https://doi.org/10.1074/jbc.C300270200

Obermeyer S, Kapoor H, Markusch H, Grasser KD. Transcript elongation by RNA polymerase II in plants: factors, regulation and impact on gene expression. Plant Journal. 2023. https://doi.org/10.1111/tpj.16115

Obermeyer S, Schrettenbrunner L, Stöckl R, Schwartz U, Grasser KD. Different elongation factors distinctly modulate RNA polymerase II transcription in *Arabidopsis*. Nucleic Acids Res. 2023:**51**(21): 11518–11533. https://doi.org/10.1093/nar/gkad825

Obermeyer S, Stöckl R, Schnekenburger T, Moehle C, Schwartz U, Grasser KD. Distinct role of subunits of the *Arabidopsis* RNA polymerase II elongation factor PAF1C in transcriptional reprogramming. Front Plant Sci. 2022:**13**:974625. https://doi.org/10.3389/fpls.2022.974625

Oh S, Park S, van Nocker S. Genic and global functions for Paf1C in chromatin modification and gene expression in *Arabidopsis*. PLoS Genet. 2008:**4**(8):e1000077. https://doi.org/10.1371/journal.pgen.1000077

Oh S, Zhang H, Ludwig P, van Nocker S. A mechanism related to the yeast transcriptional regulator Paf1c is required for expression of the *Arabidopsis* FLC/MAF MADS box gene family. Plant Cell. 2004:**16**(11):2940–2953. https://doi.org/10.1105/tpc.104.026062

Park S, Oh S, Ek-Ramos J, van Nocker S. PLANT HOMOLOGOUS TO PARAFIBROMIN is a component of the PAF1 complex and assists in regulating expression of genes within H3K27ME3-enriched chromatin. Plant Physiol. 2010:**153**(2):821–831. https://doi.org/10.1104/pp.110.155838

Quinlan AR. BEDTools: the Swiss-Army tool for genome feature analysis. Current Protocols in Bioinformatics. 2014:**47**:11.12.1-34. https://doi.org/10.1002/0471250953.bi1112s47

Rahl PB, Lin CY, Seila AC, Flynn RA, McCuine S, Burge CB, Sharp PA, Young RA. c-Myc regulates transcriptional pause release. Cell. 2010:**141**(3):432–445. https://doi.org/10.1016/j.cell.2010.03.030

Ramírez F, Dündar F, Diehl S, Grüning BA, Manke T. DeepTools: a flexible platform for exploring deep-sequencing data. Nucleic Acids Res. 2014:**42**(W1):187–191. https://doi.org/10.1093/nar/gku365

Rondón AG, Gallardo M, García-Rubio M, Aguilera A. Molecular evidence indicating that the yeast PAF complex is required for transcription elongation. EMBO Rep. 2004:**5**(1):47–53. https://doi.org/10.1038/sj.embor.7400045

Roudier F, Ahmed I, Bérard C, Sarazin A, Mary-Huard T, Cortijo S, Bouyer D, Caillieux E, Duvernois-Berthet E, Al-Shikhley L, et al. Integrative epigenomic mapping defines four main chromatin states in *Arabidopsis*. EMBO Journal. 2011:**30**(10):1928–1938. https://doi.org/10.1038/emboj.2011.103

Schmitz RJ, Tamada Y, Doyle MR, Zhang X, Amasino RM. Histone H2B deubiquitination is required for transcriptional activation of FLOWERING LOCUS C and for proper control of flowering in *Arabidopsis*. Plant Physiol. 2009:**149**(2):1196–1204. https://doi.org/10.1104/pp.108.131508

Shi X, Chang M, Wolf AJ, Chang CH, Frazer-Abel AA, Wade PA, Burton ZF, Jaehning JA. Cdc73p and Paf1p are found in a novel RNA polymerase II-containing complex distinct from the Srbp-containing holoenzyme. Mol Cell Biol. 1997:**17**(3):1160–1169. https://doi.org/10.1128/MCB.17.3.1160

Tarasov A, Vilella AJ, Cuppen E, Nijman IJ, Prins P. Sambamba: fast processing of NGS alignment formats. Bioinformatics. 2015:**31**(12): 2032–2034. https://doi.org/10.1093/bioinformatics/btv098

Vos SM, Farnung L, Boehning M, Wigge C, Linden A, Urlaub H, Cramer P. Structure of activated transcription complex Pol II–DSIF–PAF–SPT6. Nature. 2018:**560**(7720):607–612. https://doi.org/10.1038/s41586-018-0440-4

Vos SM, Farnung L, Linden A, Urlaub H, Cramer P. Structure of complete Pol II–DSIF–PAF–SPT6 transcription complex reveals RTF1 allosteric activation. Nature Structural and Molecular Biology. 2020:**27**(7):668–677. https://doi.org/10.1038/s41594-020-0437-1

Wang H, Fan Z, Shliaha P V, Miele M, Hendrickson RC, Jiang X, Helin K. H3k4me3 regulates RNA polymerase II promoter-proximal pause-release. Nature. 2023:**615**(7951):339–348. https://doi.org/10.1038/s41586-023-05780-8

Wang M, Zhong Z, Gallego-Bartolomé J, Li Z, Feng S, Kuo HY, Kan RL, Lam H, Richey JC, Tang L, et al. A gene silencing screen uncovers diverse tools for targeted gene repression in *Arabidopsis*. Nat Plants. 2023:**9**(3):460–472. https://doi.org/10.1038/s41477-023-01362-8

Wood A, Schneider J, Dover J, Johnston M, Shilatifard A. The Paf1 complex is essential for histone monoubiquitination by the Rad6-Bre1 complex, which signals for histone methylation by COMPASS and Dot1p. J Biol Chem. 2003:**278**(37):34739–34742. https://doi.org/10.1074/jbc.C300269200

Wu L, Li L, Zhou B, Qin Z, Dou Y. H2b ubiquitylation promotes RNA Pol II processivity via PAF1 and pTEFb. Mol Cell. 2014:**54**(6):920–931. https://doi.org/10.1016/j.molcel.2014.04.013

Yu M, Yang W, Ni T, Tang Z, Nakadai T, Zhu J, Roeder RG. RNA polymerase II-associated factor 1 regulates the release and phosphorylation of paused RNA polymerase II. Science. 2015:**350**(6266): 1383–1386. https://doi.org/10.1126/science.aad2338

Yu X, Michaels SD. The *Arabidopsis* Paf1c complex component CDC73 participates in the modification of FLOWERING LOCUS C chromatin. Plant Physiol. 2010:**153**(3):1074–1084. https://doi.org/10.1104/pp.110.158386

Zerbino DR, Johnson N, Juettemann T, Wilder SP, Flicek P. WiggleTools: parallel processing of large collections of genome-wide datasets for visualization and statistical analysis. Bioinformatics. 2014: **30**(7):1008–1009. https://doi.org/10.1093/bioinformatics/btt737

Zhang H, Li X, Song R, Zhan Z, Zhao F, Li Z, Jiang D. Cap-binding complex assists RNA polymerase II transcription in plant salt stress response. Plant Cell and Environment. 2022:**45**(9):2780–2793. https://doi.org/10.1111/pce.14388

Zhang H, Ransom C, Ludwig P, Van Nocker S. Genetic analysis of early flowering mutants in *Arabidopsis* defines a class of pleiotropic developmental regulator required for expression of the flowering-time switch FLOWERING LOCUS C. Genetics. 2003:**164**(1):347–358. https://doi.org/10.1093/genetics/164.1.347

Zhang H, Van Nocker S. The vernalization independence 4 gene encodes a novel regulator of FLOWERING LOCUS C. Plant Journal. 2002: **31**(5):663–673. https://doi.org/10.1046/j.1365-313X.2002.01380.x

Zhang Y, Liu T, Meyer CA, Eeckhoute J, Johnson DS, Bernstein BE, Nussbaum C, Myers RM, Brown M, Li W, et al. Model-based analysis of ChIP-Seq (MACS). Genome Biol. 2008:**9**(9):R137. https://doi.org/10.1186/gb-2008-9-9-r137

Zhao F, Xue M, Zhang H, Li H, Zhao T, Jiang D. Coordinated histone variant H2A.Z eviction and H3.3 deposition control plant thermomorphogenesis. New Phytologist. 2023:**238**(2):750–764. https://doi.org/10.1111/nph.18738